

Received April 23, 2018; reviewed; accepted June 20, 2018

## Effect of pyrite type on the electrochemistry of chalcopyrite/pyrite interactions

Elizaveta Forbes, Leanne Smith, Mikko Vepsäläinen

CSIRO Mineral Resources, Clayton, VIC 3168, Australia

Corresponding author: [liza.burdukova@gmail.com](mailto:liza.burdukova@gmail.com) (E. Forbes)

**Abstract:** Pyrite is the most common sulphide gangue mineral occurring in base metal sulphide ores around the world. Pyrite is known to galvanically interact with valuable minerals such as chalcopyrite, altering their electrochemical and flotation behaviour. Different types of pyrite are known to vary in texture, chemical composition and electrochemical activity. However, the effect that these differences have on the degree of pyrite interaction with chalcopyrite are not well studied. This work examines two distinct types of pyrite from different deposits that have a similar chemical composition, but vary greatly in texture. It investigates the way in which these pyrites interact with chalcopyrite surfaces, affecting both its electrochemical behaviour and floatability. It was found that the Renison pyrite was characterised by a much higher level of surface activity than the Huanzala pyrite. This was attributed to the elevated levels of arsenic within the mineral's crystalline matrix.

**Keywords:** pyrite, flotation, arsenic, surface oxidation, galvanic interactions

### 1. Introduction

Pyrite ( $\text{FeS}_2$ ) is one of the most commonly occurring metal sulphide minerals, and its presence is ubiquitous in ores processed in the base metal sulphide industry. In some cases (such as the PGM and gold processing operations), the recovery of pyrite is desirable due to factors such as gold substitution into the pyrite lattice and close association with finely grained PGM bearing minerals. However, in the vast majority of cases, pyrite is seen as an undesirable gangue species.

Pyrite is highly floatable and readily enters the flotation concentrates, diluting the grade of valuable products. In addition, it is well known pyrite interacts with other base metal sulphide minerals, such as chalcopyrite. Such interactions are thought to boost pyrite floatability due to copper activation, while depressing chalcopyrite through galvanic passivation (Guy and Trahar, 1985; Trahar et al., 1994; Ekmeççi and Demirel, 1997; Hu et al., 2009; Owusu et al., 2014).

Recently, anecdotal reports from industrial mining operations seem to suggest that pyrites from different deposits are characterised by distinctly different flotation behaviour. Furthermore, it has been demonstrated that small variations in pyrite composition can account for significant differences in pyrite mineral characteristics, specifically, its chemical reactivity and its electrochemical properties (Abraitis et al., 2004; Xian et al., 2015). The electrochemistry of base metal sulphide surfaces is known to have a strong effect on the mineral surface hydrophobicity through the formation of hydrophobic oxidation products on mineral surfaces (Guy and Trahar, 1985; Trahar et al., 1994; Woods, 2003). It is therefore expected that strong variations within pyrite properties are likely to have consequences with regards to the flotation response of both pyrite and other base metal sulphide minerals that it comes into contact with during the flotation process. However, very few studies exist on the topic.

This work forms part of a larger study to determine the fundamental electrochemical drivers behind the effective removal of arsenic-bearing minerals from base metal rich ores. Within these ore bodies, minerals such as enargite and tennantite are known to coexist with both chalcopyrite and pyrite. This paper focuses on the effect that differences in pyrite type have on surface properties and subsequent

flotation characteristics of chalcopyrite. The next stage of the study would then involve evaluating these effects for both enargite and tennantite surfaces.

The objective of this paper is to study two distinctly different types of pyrite and their behaviour in the presence of chalcopyrite. The properties of the three minerals (two types of pyrite and one type of chalcopyrite) are evaluated using electrochemical, analytical and microscopy techniques. These are then compared to flotation performance.

## 2. Materials and methods

### 2.1. Materials

Two types of pyrite were used in this study: 1) Renison pyrite, sourced from Tasmania, Australia (Raymond, 1996), and 2) Huanzala pyrite, sourced from Peru (Murakami et al., 2009). Initially, the study screened four different pyrite types and found that they fell into two activity categories as evidenced by their open circuit potential (see section 3.2). A single mineral from each group was selected for both clarity and efficiency purposes.

The chalcopyrite used in this study was sourced from Mt Lyell in Australia. All samples were also mounted in conjunction with a sample of enargite as part of a larger study, however, the results pertaining to enargite will not be presented here.

### 2.2. Microprobe analysis

Representative pyrite grains were mounted in an epoxy resin in a 25 mm diameter round sample holder. Samples were then polished using successively finer diamond pastes to a final polishing size of 1  $\mu\text{m}$ . A final chemo-mechanical polishing step using colloidal silica dispersed in an alkali solution was then employed to remove any amorphous layer generated by the mechanical polishing. Finally, samples were coated with a 10 nm thick carbon film prior to analysis.

Quantitative electron microprobe analyses were performed on an electron microprobe model JEOL JXA 8500F equipped with five wavelength dispersive spectrometers (WDS) and two energy dispersive spectrometers (EDS) using an accelerating voltage of 25 kV and a beam current 120 nA. The electron beam was defocused to 10  $\mu\text{m}$  for the analyses. Approximately 50 randomly selected points on each sample were analysed. The suite of elements analysed included: Fe, As, Ni, Ag, S, Cu, Se, Co, and Zn. A synthetic pyrite was analysed to determine the X-ray background shape for the trace elements and hence their offsets. X-ray lines, counting times on the peak and background, calculated  $2\sigma$  detection limits, and standards used for the elements analysed are given in Table 1. The JEOL 8500F software has been modified to allow negative k-ratios to be collected and tracked. This enables an unbiased trace element level to be calculated and the statistical scatter around zero, when an element is not present, maintained. A modern PRZ matrix correction implemented offline using a STRATAGem software was employed.

A map was collected on the Renison sample at 25kV, 80nA and a step size of 1 micron. The map was 800  $\times$  800 microns with a 100 ms dwell time per pixel. Elements mapped by WDS were As, Fe, Zn and Pb, and spectral EDS was acquired in parallel.

Table 1. Quantitative microprobe analysis conditions

Element	Line	Peak (s)	Crystal	$2\sigma$ detection limit (ppm)	Standard
Fe	Ka	8	LIF	390	Pyrite ( $\text{FeS}_2$ )
As	La	60	TAP	160	GaAs
Ni	Ka	40	LIFH	30	Heazlewoodite ( $\text{Ni}_3\text{S}_2$ )
Ag	La	100	PETJ	50	Ag metal
S	Ka	8	PETJ	655	Pyrite ( $\text{FeS}_2$ )
Cu	Ka	30	LIF	320	Chalcopyrite ( $\text{CuFeS}_2$ )
Se	La	50	TAP	85	Se metal
Co	Kb	60	LIFH	120	Co metal
Zn	Ka	30	LIF	460	Sphalerite ( $\text{ZnS}$ )

### 2.3. Microprobe analysis

All electrochemical measurements were performed using the BioLogic M470 acSECM instrument. The measurements were performed using the Saturated Calomel Electrode (SCE) as a reference electrode, and Pt wire as a counter electrode. All measurements were performed in a solution of  $10^{-2}$  M NaCl, adjusted to pH 10 using laboratory grade NaOH.

#### 2.3.1. Sample preparation

Each mineral particle was fitted with a copper cable using conductive silver epoxy, as shown in Fig. 1. The three mineral particles were then mounted in a single epoxy resin block to enable simultaneous measurement. The surface areas of each mineral particle were estimated using image analysis, with the results presented in Table 2. Prior to each electrochemical measurement, the samples were freshly polished on first 1200 calibre grit paper, followed by 6  $\mu$ m grit paper in the presence of the test solution. This technique allowed for a fresh mineral surface to be generated for each test using the same sample.

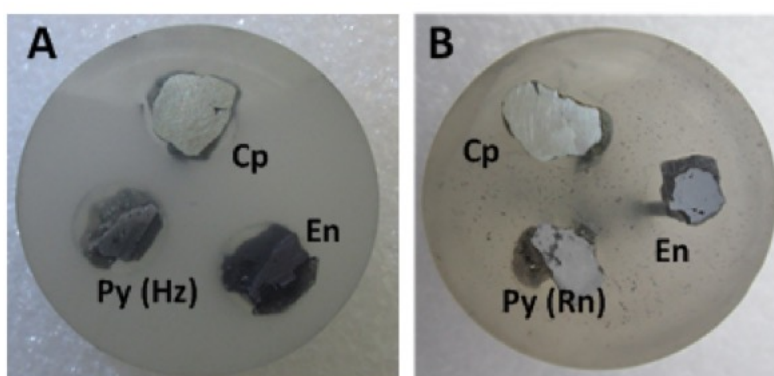


Fig. 1. Mineral electrodes used in this study

Table 2. Mineral electrode surface areas

Mineral Type	Surface Area (cm <sup>2</sup> )
Chalcopyrite (Electrode A)	0.37
Chalcopyrite (Electrode B)	0.46
Huanzala Pyrite	0.13
Renison Pyrite	0.27

#### 2.3.2. Equilibrium Open Circuit Potential measurements

Equilibrium open circuit potentials (OCP) of each electrode and electrode couples were measured for 30 minutes. The electrode potential readings for the last 10 minutes were averaged to calculate the equilibrium OCP for each condition. OCP measurements for each condition were repeated in triplicate. The average OCP values for each condition were then calculated, along with the corresponding 95% confidence limit of the mean values.

Please note that throughout this paper, all electrochemical potential values are quoted in millivolts vs. Standard Hydrogen Electrode (SHE), but for the sake of brevity will be referred to as simply millivolts (mV).

#### 2.3.3. Electrochemical Impedance Spectroscopy (EIS) measurements

The impedance ( $Z$ ) measurements were made as a function of frequency ( $f$ ), in the range between 100 kHz and 0.1 Hz. In each case, the samples were first conditioned for 900 s at the potential corresponding to the previously determined mean OCP value for the specific test condition. The conditioning potential value was then further maintained for the duration of the measurement. Under these conditions, the impedance of mineral surfaces corresponded to the natural degree of oxidation of these surfaces within the chemical conditions imposed by the aqueous solution medium.

The tests for each condition were replicated between 3 and 6 times, depending on the spread of the data. The real and imaginary components of  $Z(f)$  ( $Z'$  and  $Z''$ , respectively) were plotted against one another in the form of a Nyquist plot. The resulting data sets were analysed using Bio-Logic EC-Lab V11 software to determine the equivalent circuit parameters. The average values of the resulting circuit parameters for each test condition were then calculated, along with the corresponding 95% confidence limit of the average values.

**2.3.4. Equivalent circuit modelling**

There are a great number of different types of circuit equivalents that can be used to ensure a good fit with the experimental data (Mendiratta, 2000). However, due to the simplified nature of the experimental setup, a very basic equivalent circuit diagram was used for modelling purposes, where the three circuit parameters corresponded to the physical phenomena involved in mineral oxidation.

The oxidation process involves the transfer of an electron from the surrounding solution to the mineral surface, where it can take part in a chemical reaction with that surface. According to DLVO theory (Derjaguin and Landau, 1941; Verwey and Overbeek, 1948), the electron would need to first pass through the bulk solution, followed by the double layer surrounding the surface, finally reacting with the surface itself (Fig. 2).

Therefore, the three circuit parameters that were deemed to correspond to this physical system were: electrolyte resistance ( $R_U$ ), double layer capacitance ( $C_{DL}$ ) and resistance to surface electron transfer ( $R_{ET}$ ).

These circuit parameters would then correspond to the following equivalent circuit model (shown in Fig. 3), with the associated mathematical model for calculating the circuit parameter values shown in Equation 1:

$$Z(f) = R_U + \frac{R_U}{R_{ET} \cdot C_{DL} \cdot (i\pi f)^{\alpha+1}} \tag{1}$$

The equation corresponding to the chosen circuit model and its fit of the raw impedance data was provided by the fitting module of the EC-Lab software by Bio-Logic.

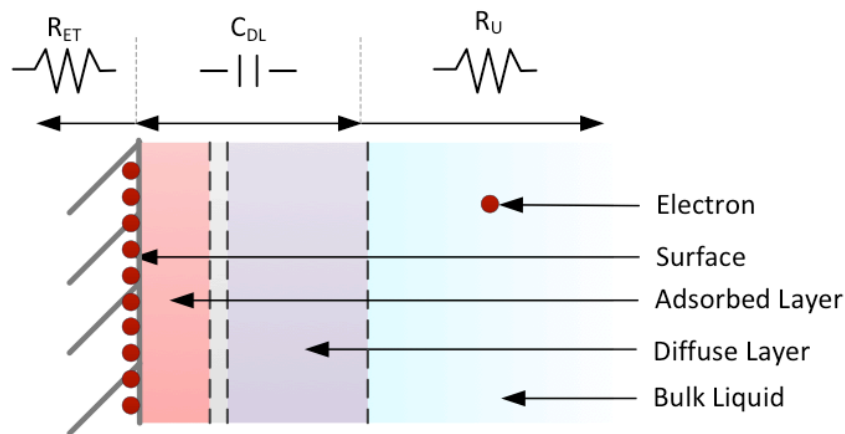


Fig. 2. Circuit equivalents for electron transfer through the electrical double layer to the mineral surface

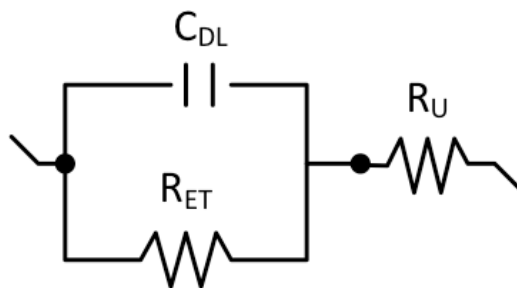


Fig. 3. Equivalent circuit model

In this simplified system, the solution conditions were kept constant. Therefore, the  $R_U$  values are expected to remain constant within the bounds of experimental error. The properties of the electrical double layer depend on two parameters: the ionic strength of the bulk solution and the electrochemical potential (or charge) of the surface itself. Since the electrolyte solution was kept consistent throughout the experiments, the differences in the calculated double layer capacitance ( $C_{DL}$ ) values are expected to be due to the differences in the mineral surface charge.

Finally, the magnitude of the resistance to the surface electron transfer ( $R_{ET}$ ) then corresponds to the degree of activity of the mineral surface and its resistance to oxidation. A high  $R_{ET}$  would then correspond to a relatively passive surface, not prone to oxidation. On the other hand, a low  $R_{ET}$  value would correspond to an active surface that readily oxidises.

## 2.4. Flotation tests

### 2.4.1. Mineral samples

Pyrite (Py) and chalcopyrite (Cp) samples were separated from high grade ore by hand picking. The upgraded portion was then stage crushed in a laboratory jaw crusher to pass 10 mesh (1.65 mm) and screened at 65 mesh (212  $\mu\text{m}$ ) to remove fines. High quality quartz obtained locally and prepared in a similar manner to the pyrite and chalcopyrite samples was used as the gangue mineral in all flotation tests.

Charges of 50 g (for single mineral tests) and 25 g (for multiple mineral tests) were riffled from each of the bulk samples for flotation testing. It is known that metal hydroxides produced from oxidation of the mineral surfaces interfere with the floatability of sulphides. To eliminate the possible effects of any hydroxides on the self-induced floatability of chalcopyrite and pyrite in this flotation study, the sulphide mineral charge was washed with 50 mL of a 1% solution of the tri-sodium salt of ethylene diamine tetra-acetic acid (EDTA) and rinsed 3 times with distilled water before grinding to remove any such oxidation products.

### 2.4.2. Reagents

All tests were conducted in the absence of collector. The EDTA used was laboratory grade. The frother used was a commercial polypropylene glycol prepared as a 0.25% w/v solution. Frother solution was added continually at a rate of 5  $\text{mg min}^{-1}$  from one minute prior to flotation to maintain an active froth. Dilute sodium hydroxide solutions were used to adjust the pH. All water was distilled and the flotation gas was high purity synthetic air used at a flow rate of 8  $\text{dm}^3 \text{min}^{-1}$ .

### 2.4.3. Grinding

For each flotation test, 50 g of sulphide mineral (either 50 g of one mineral only in single mineral tests or 25 g of chalcopyrite and 25 g of the pyrite of choice in mixed mineral tests) and 450 g of quartz were ground for 20 minutes in a stainless steel ball mill at a solid-liquid ratio of 2:1 (i.e. 67% solids by weight). A stainless steel rather than iron mill was used to avoid the reducing conditions of closed iron mills.

### 2.4.4. Flotation procedure

The flotation tests were performed in a 3 L modified Denver cell (Guy, 1992) in which the impeller was driven from below to allow the whole surface of the froth to be scraped with a paddle at a constant depth and at constant time intervals. The cell was fitted with a rubber diaphragm, sight tube and electronic sensor for automatic detection and control of the pulp level.

The ground pulp was put in the flotation cell, the pH adjusted to pH 10 and the pulp level made up to the set level. The pulp was then aerated for 5 minutes to ensure the pulp potential was at the air set potential (approximately 280 mV). The pulp potential and pH were monitored continuously throughout the tests. Potentials were measured with a polished platinum flag electrode using a Ag/AgCl reference and converted to the standard hydrogen electrode (SHE) scale by the addition of 0.2 V. A combination glass/red rod pH electrode was used to monitor the pH.

One minute before flotation, the air was turned off and frother addition commenced. Concentrates were taken after 0.5, 1, 2, 4 and 8 minutes. The froth was scraped every 2 s for the first minute of flotation and every 5 s thereafter. Flotation products were weighed both wet (to allow calculation of water recoveries) and dry, and were prepared for analysis in a standard manner.

#### 2.4.5. Elemental analysis

Flotation products were assayed for copper, iron and sulphur by inductively coupled plasma (ICP) optical emission spectrometry. The flotation behaviour of chalcopyrite in mixed mineral tests was determined from the copper assays and the flotation behaviour of pyrite was calculated from the sulphur assays with allowance for the sulphur present as chalcopyrite.

### 3. Results and discussion

#### 3.1. Mineral properties and composition

##### 3.1.1. Surface SEM images

The surfaces of the two pyrites were analysed using scanning electron microscopy (SEM) imaging, with the results presented in Fig. 4. The figure shows both Huanzala (A) and Renison (B) pyrite surfaces at two magnification levels. The figure clearly indicates that the surface of Huanzala pyrite is extremely smooth and free of features. In contrast, Renison pyrite displays a rough and pitted texture, with a number of inclusions. This is consistent with the description of Renison pyrite in other publications (Raymond, 1996).

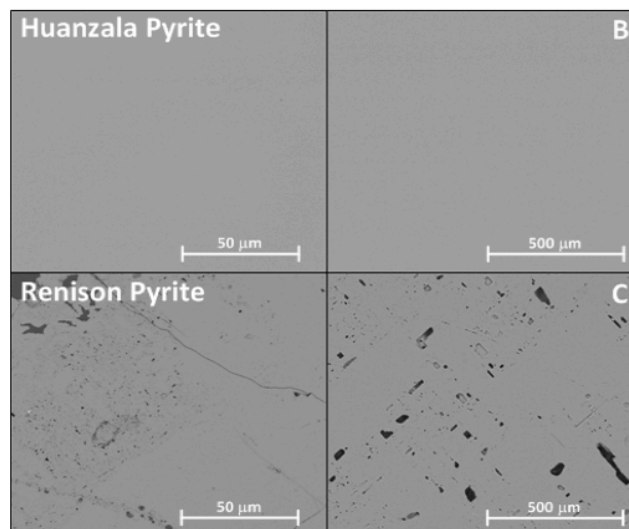


Fig. 4. SEM analysis of A) Huanzala and B) Renison pyrite surfaces at different levels of magnification

##### 3.1.2. Pyrite composition

A more detailed analysis of the composition of the two pyrites was conducted using microprobe analysis, summarised in Table 3. The chemical composition of both pyrites is also very similar, displaying a S:Fe ratio of 1.16 and 1.20 for Huanzala and Renison pyrites respectively, indicating both pyrite types fall into the n-pyrite category (S:Fe ratio of < 2). This makes them similar to the pyrite samples tested in other studies ((Abraitis et al., 2004; Doyle and Mirza, 1996). The results also show that Renison pyrite contains large quantities of arsenic, at levels that are an order of magnitude larger than those found in Huanzala pyrite.

In order to determine the source and distribution of arsenic throughout the Renison pyrite mineral, a map of As concentrations was performed on the Renison pyrite surface, with additional As concentration measured at three different points, as summarised in Fig. 5 and Table 4.

A map of the Renison pyrite sample showed strong As zoning. The dark grains in the map are fluorine-rich apatites. The As zoning appears to reflect the pyrite mineralisation that was reported by Raymond

(1996). Table 4 shows arsenic varying from very low in the dark areas through to almost 1 wt% in the elevated regions.

Table 3. Trace element analysis of the pyrite samples

Composition	Huanzala Py	Renison Py
Fe	45.8%	46.1%
S	54.2%	53.7%
As	0.01%	0.16%
Ni	0.00%	0.00%
Ag	0.00%	0.00%
Cu	0.01%	0.01%
Se	0.01%	0.01%
Co	0.00%	0.00%
Zn	0.02%	0.02%
<b>TOTAL</b>	100%	100%

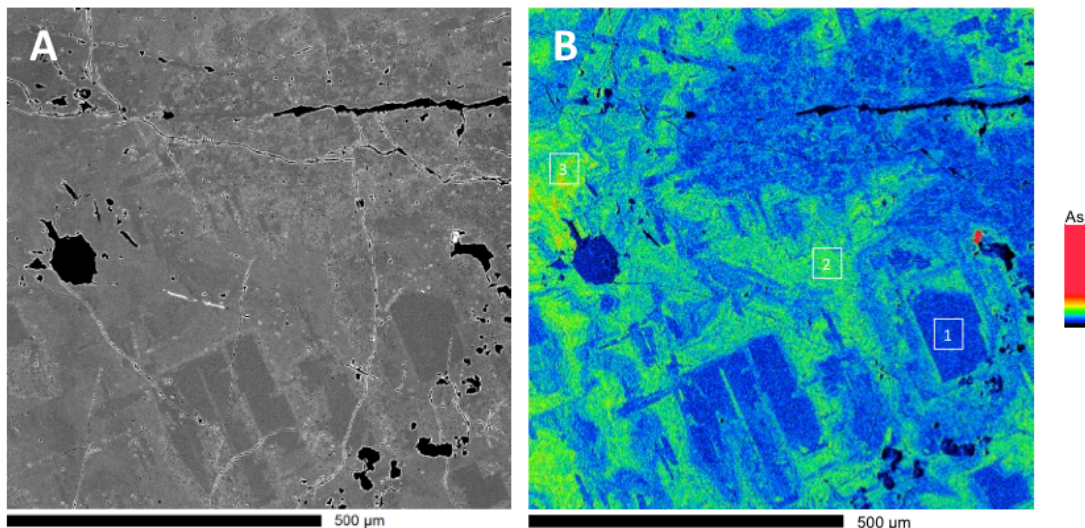


Fig. 5. (A) Backscattered electron map and (B) As map of the Renison pyrite surface

Table 4. Quantitative analysis points recorded across the Renison pyrite mapped section, as shown in Fig. 4

Point Number	Fe	As	Ni	Ag	S	Cu	Se	Zn	Total
1	46.2%	0.022%	0.002%	0.004%	51.4%	0.001%	0.018%	0.047%	98%
2	46.0%	0.814%	0.000%	0.001%	53.1%	0.027%	0.032%	0.025%	100%
3	46.8%	0.930%	0.003%	0.000%	52.4%	0.009%	0.045%	0.044%	100%

Various analytical methods have demonstrated that the two pyrite minerals contained significantly different levels of arsenic (See Table 3). The As content of pyrite can be elevated for two reasons. One is the presence of fine arsenopyrite (FeAsS) inclusion, while the other is substitutions of As into the pyrite crystal structure, forming arsenian pyrite. Arsenian pyrite can in turn be formed by two kinds of substitutions. One is the substitution of  $\text{As}^{-1}$  for S in the pyrite matrix  $[\text{Fe}(\text{As}^{-1}\text{-S})_2]$  (Fleet and Mumin, 1997), while the other is the substitution of  $\text{As}^{3+}$  for Fe  $[(\text{Fe,As})\text{S}_2]$  (Deditius et al., 2008).

Cruz et al. (2001) cited six different pyrites, with As content ranging from 0.02 to 1.18 %, where As levels above 0.06% were attributed to arsenopyrite inclusions within the main pyrite matrix. Abratis et al. (2004) reviewed ten different types of pyrite (including arsenian pyrite) which varied between 6 ppm

and 9.6 wt%, while Deditius et al. (2008) quoted As concentrations between 0.08 and 3.5 wt% for arsenian pyrite.

Overall, while the As levels within Renison pyrite are high (0.16%), they fall within the measured range of concentrations within arsenian pyrites. Furthermore, the distribution of As throughout the Renison pyrite matrix (as seen in Fig. 4), as well as the nature of its geological formation (Raymond, 1996), strongly suggests that the presence of arsenic within this mineral is due to substitution of As ions within the mineral matrix. At this point it is not clear whether the As is substituting with  $\text{Fe}^{3+}$  ions (in the form of  $\text{As}^{3+}$ ) or for S (in the form of  $\text{As}^{1-}$ ).

On the other hand, Huanzala pyrite contains very low levels of As (0.01%), and contains very low levels of other impurities. The SEM images of this mineral (see Fig. 4 A) show a mirror smooth mineral surface. This mineral can therefore be considered a “model” natural pyrite.

### 3.2. Open circuit potential measurements

Different mineral types also have a tendency to have a specific natural or rest electrode potential under specific chemical conditions (such as pH). Such open circuit potential (OCP) values were measured for chalcopyrite, Renison pyrite and Huanzala pyrite electrodes at pH 10. The OCP values for electrode pairs were similarly measured, with the results presented in Fig. 6.

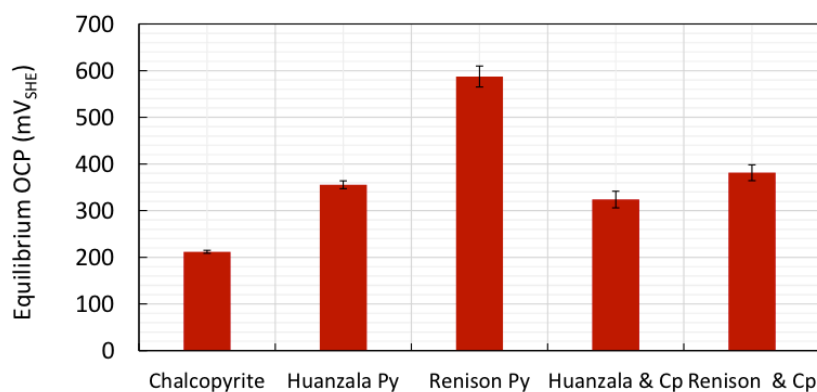


Fig. 6. Equilibrium open circuit potential measurements for pure minerals and mineral couples, error bars represent the 95% confidence interval of the mean

#### 3.2.1. Single minerals

All three minerals tested showed significant differences in their open circuit potential measurements (note that all error values represent the 95% confidence interval of the mean value). The OCP of chalcopyrite produced an average of  $211 \pm 3$  mV, which is consistent with similar measurements reported in other studies (Owusu et al., 2013; Owusu et al., 2014). The average OCP of Huanzala pyrite was  $355 \pm 8$  mV, while that for Renison pyrite was  $587 \pm 22$  mV. The measured difference between the two types of pyrite is highly unusual and in contradiction with a number of studies.

Doyle and Mirza (1996) tested the rest potentials of twelve different types of pyrite in highly acidic conditions (0.1 M  $\text{H}_2\text{SO}_4$ ). They found very little variation between them, with the measurements falling in the range between 558 and 699 mV, the average resting at 647 mV. Similarly, Cruz et al. (2001) tested six different pyrites at pH 6.5, with OCP values ranging from 325 to 345 mV. Both sets of researchers concluded pyrite OCP was not sensitive to pyrite composition, which included significant differences in arsenic content. The main difference between this study and those by other authors is that it was conducted in an alkaline pH range (consistent with flotation conditions in most mining operations). It is possible that under alkaline conditions (pH 10), the differences in pyrite composition come to the fore and hence have a larger effect on mineral potential.

The effect of mineral potential on the self-induced flotation of sulphide minerals has been well established (Ekmekçi and Demirel, 1997; Guy and Trahar, 1985; Woods, 2003). Sufficiently high natural or applied electrode potential causes the surfaces of sulphide minerals to oxidise. The oxidation process typically results in the formation of highly hydrophobic elemental sulphur species on the mineral

surfaces, rendering them naturally floatable. Different minerals oxidise at different electrochemical potential levels, something that has been explored to obtain selective flotation and/or depression of minerals (Heyes and Trahar, 1979; Luttrell and Yoon, 1984; Owusu et al., 2014; Richardson et al., 1984). It is therefore expected that the difference in the OCP of the two pyrites in question will be corroborated by the difference in natural floatability of these minerals.

### 3.2.2. Galvanic pairs

The OCP values for the two Cp/Py galvanic couples exhibit small, but significant differences ( $323 \pm 17$  mV and  $381 \pm 17$  mV for Huanzala and Renison pyrites, respectively), and are due to the galvanic interactions between chalcopyrite and pyrite. Within such a pairing, pyrite is the nobler electrode (characterised by the higher rest potential) and will act as a cathode in the galvanic interaction, whereas chalcopyrite will act as the anode. Such a galvanic interaction would then enhance the oxidation rate on the chalcopyrite surface, forming elemental sulphur and CuS species, whereas the cathodic reaction on the pyrite surfaces would reduce ferric hydroxide to ferrous hydroxide (Ekmekçi and Demirel, 1997). It is expected that the significantly higher potential of Renison pyrite compared to Huanzala pyrite would enhance the galvanic interaction. However, the electrode reactions of the galvanic couple are also influenced by the surface area ratios of minerals, which were not same in the Cp-Huanzala and Cp-Renison pairs. The Cp:Py surface area ratios for Cp-Huanzala and Cp-Renison pairs were 2.84 and 1.71, respectively. This means that the influence of Renison pyrite on the galvanic coupling was significantly reduced compared to that of Huanzala pyrite. This in turn means that although the final OCP values of the two galvanic pairings were similar, Huanzala pyrite had a significantly weaker influence on the galvanic chalcopyrite/pyrite pairing than the Renison pyrite. These findings lead to an expectation that the flotation of chalcopyrite in the presence of Renison pyrite would differ from that in the presence of Huanzala pyrite.

### 3.3. Electrochemical impedance spectroscopy (EIS) measurements

Once the open circuit potentials of the three minerals and their pairings had been established, the matching EIS measurements were performed. It is important to note that prior to and during the EIS measurements, the electrical potential was maintained at the corresponding OCP measurements presented in Fig. 6.

#### 3.3.1. Equivalent circuit model

For each test condition, the real ( $Z'$ ) and imaginary ( $Z''$ ) components of the impedance spectra were plotted on a Nyquist diagram and fitted with the equivalent circuit model, as shown in Fig. 7. The model takes the form of a semicircle, where the values of the uncompensated background electrolyte resistance ( $R_U$ ) and resistance to electron transfer ( $R_{ET}$ ) can be calculated from the two x intercept values. The average  $R_{ET}$  values obtained for the minerals and mineral couples are presented in Fig. 8.

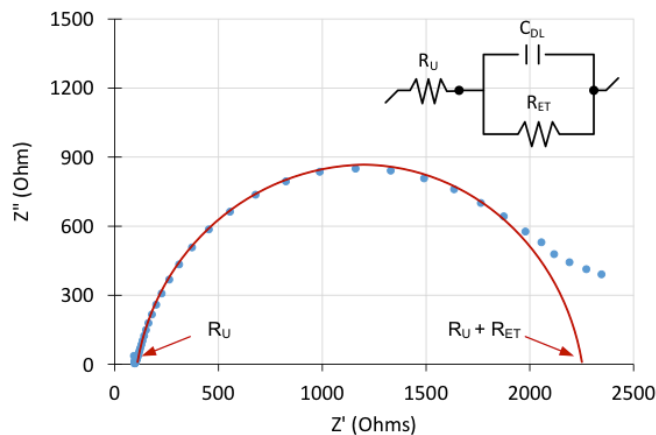


Fig. 7. Example of a Nyquist diagram (data for a test using Renison pyrite, at a potential of 587 mV) being fitted with the equivalent circuit model

Fig. 7 demonstrates that the impedance data measured for this system of electrodes corresponds well to similar measurements made in such systems available in literature (Hu et al., 2009). It also shows that the circuit model (Equation 1) is a reasonably good fit for the experimental data over the majority of the measured range.

A summary of all the calculated electron transfer resistance ( $R_{ET}$ ) values is presented in Fig. 8. It must be noted that a significant amount of variation was detected between repeated measurements for the same conditions, which are reflected in the 95% confidence interval error bars. Such a high degree of variation likely results from the fact that the samples were freshly polished before each measurement. The act of polishing has previously been blamed for similar variations in other studies (Mendiratta, 2000). However, despite the high degree of variation, the differences in the  $R_{ET}$  values can still be considered significant.

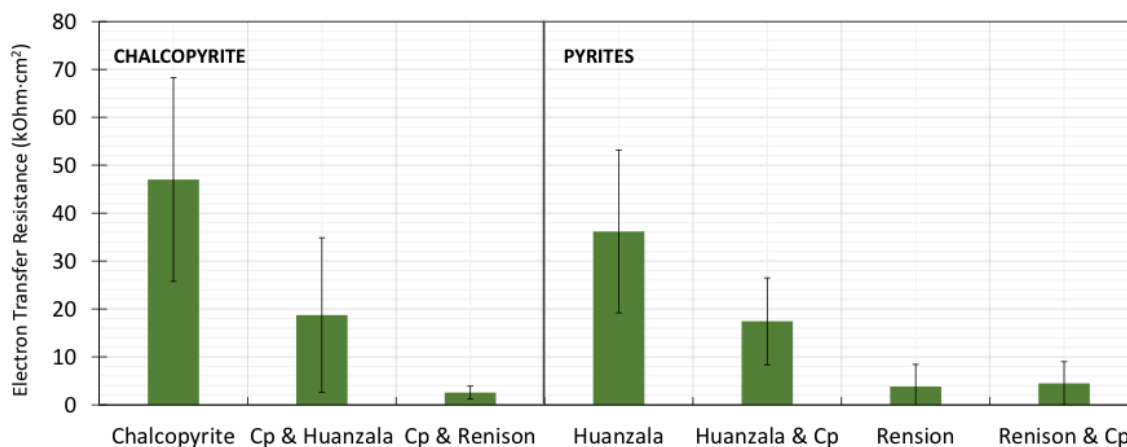
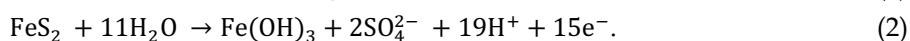


Fig. 9. Electron transfer resistance ( $R_{ET}$ ) values derived from Nyquist plots for pure minerals and mineral couples, error bars represent the 95% confidence interval of the mean

### 3.3.2. Single minerals

The results demonstrate that the  $R_{ET}$  values for chalcopyrite and Huanzala pyrite were similar ( $47 \pm 21$  and  $36 \pm 17$  kOhm cm<sup>2</sup>, respectively), indicating a similar level of surface activity. On the other hand, the  $R_{ET}$  value for Renison pyrite was significantly lower, at  $4 \pm 5$  kOhm cm<sup>2</sup>, indicating a much higher level of surface activity than both chalcopyrite and Huanzala pyrite.

The elevated activity of Renison pyrite, coupled with elevated arsenic concentrations, is in full agreement with other authors, who have all stated that arsenic rich pyrites are characterised by higher levels of chemical activity (Abraitis et al., 2004; Cruz et al., 2001; Deditius et al., 2008; Doyle and Mirza, 1996). The oxidation of pyrite can be interpreted in terms of the following reactions (Hamilton and Woods, 1981):



In cases where Reaction 2 is dominant, the oxidation reaction produces elemental sulphur on the pyrite surface, rendering in hydrophobic. However, if Reaction 3 is dominant, the oxidation products deposited on the pyrite surface are iron hydroxide and sulphony species, leading to a hydrophilic surface. According to Pourbaix diagrams of sulphur and its complexes (Chen et al., 2016), the formation of elemental sulfur is very limited at pH 10, thus making Reaction 3 the dominant reaction under these conditions. The exact nature of the surface speciation of pyrite cannot be determined without an in-depth surface analysis and will not be further speculated upon in this paper.

Although a number of researchers claim that the presence of arsenic within the pyrite increases its activity, no information is provided as to how this affects the pyrite oxidation reactions. One can speculate that if  $\text{As}^{3+}$  is substituting in for  $\text{Fe}^{3+}$  ions in the pyrite matrix (Deditius et al., 2008), it would weaken the mineral surface structure through a bond-length mismatch between arsenic and sulphur atoms. Such a weakening could then result in an enhanced leaching of elemental sulphur ( $\text{S}^0$ ) upon

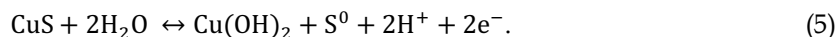
oxidation. However, a more detailed study involving the oxidation products of the two pyrites (using a technique such as XPS) would be required to determine the exact reaction.

### 3.3.3. Galvanic pairs

The results in Fig. 8 show that the galvanic interaction between the chalcopyrite and pyrite samples significantly suppressed the charge transfer resistance ( $R_{ET}$ ) of the chalcopyrite electrodes. This indicates an enhanced reaction rate on the surface, which in this system would be the oxidation of the mineral according to Equation 4 (Gardner and Woods, 1979):



Further oxidation of the CuS may occur according to Equation 5:



According to Ekmekçi and Demirel, (1997), the corresponding potential reduction reactions of pyrite through galvanic interaction with chalcopyrite consist of the reduction of sulphate to form sulphides, the reduction of oxygen and the reduction of ferric ions to form ferrous complexes.

Renison pyrite had a significantly stronger effect on the chalcopyrite charge transfer resistance value than Huanzala pyrite ( $2.5 \pm 1$  vs.  $19 \pm 16$  kOhm cm<sup>2</sup>, respectively). The results are supported by the OCP values, according to which Renison pyrite is nobler and had stronger galvanic effect with the chalcopyrite.

### 3.4. Flotation tests

The results of the flotation tests are shown in Figs 9 and 10 in the form of recovery-time plots. From the curves for the single sulphide mineral tests in the absence of collector, it can be seen that chalcopyrite is strongly floatable at pH 10 while both pyrites are poorly floatable. This is in line with other published results (Ekmekçi and Demirel, 1997; Trahar et al., 1994) of the flotation of chalcopyrite and pyrite in the absence of collectors.

Pyrite flotation in the presence of chalcopyrite was still poor. The floatability of Huanzala pyrite decreased slightly in the presence of chalcopyrite but the difference was so small that it fitted well within the typical level of experimental error ( $\approx 5\%$ ) due to inconsistencies with water recovery or feed distribution. The floatability of Renison pyrite, however, increased in the presence of chalcopyrite from 4% to 13% which is probably more than could be accounted for by changes in water recovery and/or feed distribution.

The strong flotation of chalcopyrite in the absence of collector in alkaline conditions is thought to be due to the formation of elemental sulphur due to oxidation of the chalcopyrite surface, according to Reaction 4 and 5. The poor flotation of pyrite in the absence of collector in alkaline conditions is thought to be due to the dominance of Reaction 3 over Reaction 2 (Heyes and Trahar, 1984), where sulphate species are formed on pyrite surfaces instead of elemental sulphur. According to the OCP results (Fig. 6), the potential of chalcopyrite increases when it is in galvanic contact with pyrite. In this system pyrite would be the cathode of the cell and chalcopyrite the anode. From the impedance spectroscopy results, the electron transfer resistance ( $R_{ET}$ ) of chalcopyrite significantly decreases in the presence of the galvanic contact with pyrite. This would indicate a faster reaction rate on the chalcopyrite surface and hence Equations 2 and 3 would be pushed further to the right, producing higher concentrations of metal hydroxides.

The strong floatability of chalcopyrite in the absence of collector has been shown to be diminished by the presence of metal hydroxides (Guy and Trahar, 1985; Woods, 2003). Therefore it was expected that the floatability of chalcopyrite from the chalcopyrite/pyrite/quartz mixtures may be diminished as a result of increased oxidation. However, chalcopyrite flotation in the current study (Fig. 9) was not significantly affected by the presence of pyrite. There was a small decrease in the rate of chalcopyrite flotation in the presence of pyrite but overall chalcopyrite recoveries were not significantly different.

Ekmekçi and Demirel (1997) found that chalcopyrite floatability significantly decreased with an increasing Py:Cp ratio in the flotation pulp. However, at similar Cp/Py/Q proportions as in these tests, the effect of the presence of pyrite on chalcopyrite flotation was minimal.

Due to the significantly higher potential of Renison pyrite, the galvanic interaction with the chalcopyrite would be expected to be enhanced compared to Huanzala pyrite. Ekmekçi and Demirel (1997) also found that the flotation of pyrite in the absence of collector increased in the presence of chalcopyrite. Once again, the difference in both electrochemical and subsequent flotation behaviour can be partially ascribed to the elevated concentration of arsenic within the structure of Renison pyrite.

Ekmekçi and Demirel (1997) suggested two different mechanisms for the increased flotation of pyrite: (a) elemental sulphur or metal-deficient sulphur generated by the pyrite itself; or (b) copper activation of the pyrite. These mechanisms would take place as a result of the galvanic interaction between the two sulphide minerals. Normally pyrite oxidises according to Equation 3, producing sulphate ions. The first mechanism would require that in the presence of chalcopyrite, the oxidation of pyrite would be modified in such a manner as to make Equation 2 more likely.

Copper activation of pyrite was discounted by Trahar et al. (1994), as they were unable to increase the self-induced flotability of pyrite by the addition of copper ions. Trahar et al. (1994) did detail circumstances under which pyrite could be shown to exhibit self-induced flotation by the transfer of a sulphur entity from a mineral such as chalcopyrite or galena to the pyrite. Such behaviour may be governed by increased sulphur production through increased oxidation of the chalcopyrite as a result of the galvanic interaction between chalcopyrite and pyrite

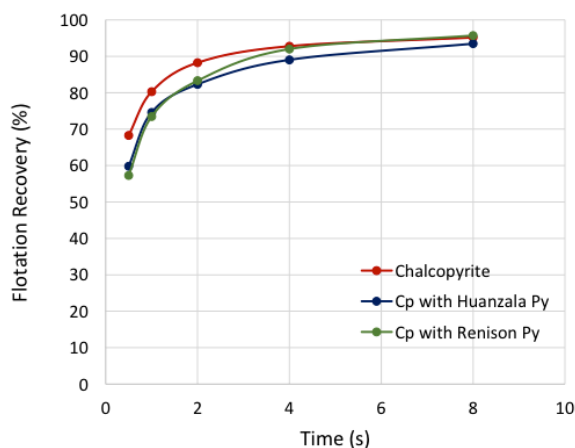


Fig. 9. Flotation recoveries for chalcopyrite, both in the presence and absence of the two pyrite types, performed at pH 10, at an air set potential of  $\approx 280 \text{ mV}_{\text{SHE}}$

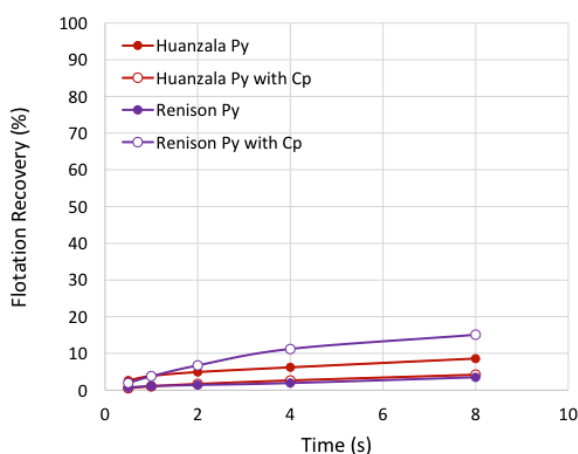


Fig. 10. Flotation recoveries for Huanzala and Renison pyrites, both in the presence and absence of chalcopyrite, performed at pH 10, at an air set potential of  $\approx 280 \text{ mV}_{\text{SHE}}$

#### 4. Implications for ARsENIC rejection

In addition to examining the effect of different types of pyrite has on chalcopyrite flotation, the findings of this work have implications for arsenic rejection by flotation. As was mentioned in the introduction,

this work forms part of a greater effort to understand the drivers and complexities behind the effective removal of arsenic-bearing minerals from base metal rich ores. This work has shown that As levels within Renison pyrite are as high as 0.16% (1600 ppm), which is close to the arsenic smelter penalty limit of 2000 ppm. Other authors have demonstrated that natural As levels within pyrite can reach as high 9 wt% (Abraitis et al., 2004). Although pyrite is typically rejected from flotation concentrates, this level of rejection is not perfect. The large quantity of pyrite in certain ore bodies (as high as 80% in some cases) means that even the low levels of recovery of pyrite into the concentrate can significantly contribute to the concentrate overall arsenic content.

## 5. Conclusions

From the information presented in this paper, the following conclusions can be drawn:

- Two pyrites were examined in this study (Renison and Huanzala pyrite). Renison pyrite was found to have significant level of arsenic within its structure (0.16%), which was an order of magnitude larger than that for Huanzala pyrite (0.01%). In addition, the two pyrites displayed clear differences in texture, where Renison pyrite was characterised by pitting and occlusions, while Huanzala pyrite was almost mirror smooth.
- Microprobe analysis of Renison pyrite identified that arsenic was distributed throughout the pyrite matrix, suggesting that the high arsenic content was caused by ion substitution (forming arsenian pyrite) rather than arsenopyrite occlusions.
- Both open circuit and EIS measurements indicated that Renison pyrite had a much higher level of electrochemical activity than Huanzala pyrite.
- Both open circuit potential and EIS measurements indicated that Renison pyrite surfaces are more affected by the galvanic interaction with chalcopyrite than Huanzala pyrite surfaces, which remain largely unchanged.
- This was confirmed by the fact that the floatability of Renison pyrite improved in the presence of chalcopyrite, while that of Huanzala pyrite remained unchanged. The increase in Renison pyrite floatability can be attributed to a greater degree of surface oxidation, which may lead to the formation of elemental sulphur species on Renison pyrite surfaces.
- The galvanic pairing of chalcopyrite with Renison pyrite had a significantly stronger effect on the open circuit potential and electrochemical impedance of chalcopyrite than Huanzala pyrite.
- The pairing with neither one of the pyrite types caused a significant shift in the floatability of chalcopyrite. Further work is necessary to investigate this effect.
- Although speculations can be made regarding the exact mechanism that of elevated arsenic content within Renison pyrite plays in increasing its surface activity, further study of oxidation products is required to determine the exact nature of the surface reactions. Such studies should be conducted using techniques such as X-ray Photoelectron Spectroscopy.
- The contribution of arsenian pyrite to the overall arsenic content of an orebody must be taken into consideration when evaluating treatment options for arsenic rejection from base metal sulphide ores.

## Acknowledgments

The authors would like to acknowledge the help and contribution of Mathew Glenn (Scanning Electron Microscopy); Colin MacRae (Microprobe analysis); Cheryl McHugh (Inductively Coupled Plasma Mass Spectrometry), and Luda Malishev and Cameron Davis for laboratory assistance.

## References

- ABRAITIS, P.K., PATTRICK, R.A.D., VAUGHAN, D.J., 2004. *Variations in the compositional, textural and electrical properties of natural pyrite: a review*. International Journal of Mineral Processing, 74(1-4), 41-59.
- CHEN, G., YANG, H., and LI, H., 2016. *In situ characterization of natural pyrite bioleaching using electrochemical noise technique*. International Journal of Minerals, Metallurgy, and Materials, 23(2): 117-126
- CRUZ, R., BERTRAND, V., MONROY, M., GONZÁLEZ, I., 2001. *Effect of sulfide impurities on the reactivity of pyrite and pyritic concentrates: a multi-tool approach*. Applied Geochemistry, 16(7), 803-819.

- DEDITIUS, A.P., UTSUNOMIYA, S., RENOCK, D., EWING, R.C., RAMANA, C.V., BECKER, U., KESLER, S.E., 2008. *A proposed new type of arsenian pyrite: Composition, nanostructure and geological significance*. *Geochimica et Cosmochimica Acta*, 72(12), 2919-2933.
- DERJAGUIN, B.V., LANDAU, L., 1941. *Theory of stability of strongly charged lyophobic sols and the adhesion of strongly charged particles in solution of electrolytes*. *Acta Physicochim*, 14, 633 - 662.
- DOYLE, F.M., MIRZA, A.H., 1996. *Electrochemical oxidation of pyrite samples with known composition and electrical properties*, In *Electrochemical Proceedings* pp. 203 - 214.
- EKMEKÇI, Z., DEMIREL, H., 1997. *Effects of galvanic interaction on collectorless flotation behaviour of chalcopyrite and pyrite*. *International Journal of Mineral Processing*, 52(1), 31-48.
- FLEET, M.E., MUMIN, A.H., 1997. *Gold-bearing arsenian pyrite and marcasite and arsenopyrite from Carlin Trend gold deposits and laboratory synthesis*. *American Mineralogist*, 82, 182-193.
- GARDNER, J.R., WOODS, R., 1979. *An electrochemical investigation of the natural flotability of chalcopyrite*. *International Journal of Mineral Processing*, 6(1), 1-16.
- GUY, P.G., 1992. *The development of laboratory batch flotation equipment and practice at CSIRO Australia*, In *AusIMM Annual Conference*. AusIMM, Melbourne, Australia, pp. 75 - 79.
- GUY, P.G., TRAHAR, W.J., 1985. *The Effects of Oxidation and Mineral Interaction on Sulfide Flotation*, In *Flotation of Sulfide Minerals*, ed. Forrsberg, E. Elsevier, pp. 63 - 71.
- HAMILTON, I.C., WOODS, R., 1981. *An investigation of surface oxidation of pyrite and pyrrhotite by linear potential sweep voltammetry*. *Journal of Electroanalytical Chemistry and Interfacial Electrochemistry*, 118, 327-343.
- HEYES, G.W., TRAHAR, W.J., 1979. *Oxidation-Reduction effects in the flotation of chalcocite and cuprite*. *International Journal of Mineral Processing*, 6(3), 229-252.
- HEYES, G.W., TRAHAR, W.J., 1984. *The flotation of pyrite and pyrrhotite in the absence of conventional collectors*, In *Electrochemistry in Minerals and Metal Processing*, eds. Richardson, P.E., Srinivasan, S., Woods, R., pp. 219-232.
- HU, Y., SUN, W., WANG, D., 2009. *Chapter 7 - Corrosive Electrochemistry of Oxidation-Reduction of Sulfide Minerals*, In *Electrochemistry of Flotation of Sulphide Minerals*. Springer-Verlag, Berlin Heidelberg, pp. 167 - 200.
- LUTTRELL, G.H., YOON, R.-H., 1984. *The collectorless flotation of chalcopyrite ores using sodium sulfide*. *International Journal of Mineral Processing*, 13(4), 271-283.
- MENDIRATTA, N.K., 2000. *Kinetic Studies of Sulfide Mineral Oxidation and Xanthate Adsorption*, In *Materials Engineering and Science*. Virginia Polytechnic Institute.
- MURAKAMI, R., YAMANAKA, K., GOMI, A., FUJII, N., 2009. *Exploration of the Huanzalà mine, Republic of Perú -The discovery of a deep mineralized zone*. *Shigen-Chishitsu* 59(2), 91-106.
- OWUSU, C., ADDAI-MENSAH, J., FORNASIERO, D., ZANIN, M., 2013. *Estimating the electrochemical reactivity of pyrite ores-their impact on pulp chemistry and chalcopyrite flotation behaviour*. *Advanced Powder Technology*, 24(4), 801-809.
- OWUSU, C., BRITO E ABREU, S., SKINNER, W., ADDAI-MENSAH, J., ZANIN, M., 2014. *The influence of pyrite content on the flotation of chalcopyrite/pyrite mixtures*. *Minerals Engineering*, 55, 87-95.
- RAYMOND, O.L., 1996. *Pyrite composition and ore genesis in the Prince Lyell copper deposit, Mt Lyell mineral field, western Tasmania, Australia*. *Ore Geology Reviews*, 10(3), 231-250.
- RICHARDSON, P.E., STOUT, J.V., PROCTOR, C.L., WALKER, G.W., 1984. *Electrochemical flotation of sulfides: Chalcocite-ethylxanthate interactions*. *International Journal of Mineral Processing*, 12(1-3), 73-93.
- TRAHAR, W.J., SENIOR, G.D., SHANNON, L.K., 1994. *Interactions between sulphide minerals – the collectorless flotation of pyrite*. *International Journal of Mineral Processing*, 40(3), 287-321.
- VERWEY, E.J.W., OVERBEEK, J.T.G., 1948. *Theory of Stability of Lyophobic Solids*. Elsevier, Amsterdam.
- WOODS, R., 2003. *Electrochemical potential controlling flotation*. *International Journal of Mineral Processing*, 72(1), 151-162.
- XIAN, Y., WANG, Y., WEN, S., NIE, Q., DENG, J., 2015. *Floatability and oxidation of pyrite with different spatial symmetry*. *Minerals Engineering*, 72, 94-100.